https://doi.org/10.5194/acp-2022-817
Preprint. Discussion started: 19 December 2022

Atmospheric Chemistry and Physics Discussions

Opposing trends of cloud coverage over land and ocean under global warming

Huan Liu[1], Ilan Koren[1], Orit Altaratz[1], Mickael D. Chekroun[1]

[1]Department of Earth and Planetary Sciences, Weizmann Institute of Science, Rehovot, 76100, Israel

Correspondence to: Ilan Koren (ilan.koren@weizmann.ac.il)

Abstract. Clouds play a key role in Earth's energy budget and water cycle. Their response to global warming contributes the largest uncertainty to climate prediction. Here, by performing an empirical orthogonal function analysis on 42 years of reanalysis data of global cloud coverage, we extract clear trend and ENSO-associated modes. The trend mode translates spatially to a decreasing trend in cloud coverage over most continents and an increasing trend over the tropical and subtropical oceans. A reduction in near-surface relative humidity can explain the decreasing trend in cloud coverage over land. Our results suggest potential stress on the terrestrial water cycle and changes in the energy partition between land and ocean, all associated with global warming.

1 Introduction

Clouds cover more than 60 % of the Earth's surface. They play a critical role in the global water cycle (Bengtsson, 2010) and act as the primary energy gatekeepers for the climate system by reflecting incoming solar radiation and blocking outgoing terrestrial radiation (Stephens et al., 2012). Overall, clouds cool the surface at a rate of approximately 20 W m^{-2} (Stephens et al., 2012).

One of the most pressing needs in climate prediction is to clarify whether and how global warming impacts clouds on a global scale and to delineate the mechanisms at play (Zelinka et al., 2020). A common practice for addressing this question consists of analyzing cloud feedbacks that can either amplify (positive feedback) or dampen (negative feedback) surface warming. However, estimating the overall cloud feedback is a challenging task since the net radiative effect depends on the type, geographical location, vertical extent, lifetime, and optical properties of clouds (Chen et al., 2000). So far, estimations of clouds' responses to the warming trend are inconclusive (Aerenson et al., 2022; Forster et al., 2021). To partly address this issue, we explore the influence of climate change on global cloud coverage, which is, of course, one of the most crucial cloud factors.

Previous works that examined trends in cloud coverage under a warmer climate show substantial discrepancies among them (Gettelman and Sherwood, 2016; Ceppi et al., 2017; Zelinka et al., 2020). Even estimations for the same cloud type vary between studied periods, locations, datasets, and models (Zhou et al., 2016; Norris et al., 2016; Karlsson and Devasthale, 2018; Zelinka et al., 2017). Important factors leading to these discrepancies are related to data uncertainties due to measurement

https://doi.org/10.5194/acp-2022-817
Preprint. Discussion started: 19 December 2022


Atmospheric Chemistry and Physics Discussions

errors in observations on the one hand (Chepfer et al., 2014), and the unsatisfactory representation of clouds in climate models on the other (Stevens et al., 2013). For example, surface observations suffer from non-uniform sampling and station migrations (Warren et al., 2007; Eastman et al., 2011), while satellite records suffer from changing view geometries and orbit drifts (Evan et al., 2007; Norris and Evan, 2015). While attempts are being made to correct some of these issues, the corrected products may remove actual cloud tendencies at a global scale (Norris and Evan, 2015; Norris et al., 2016). As for climate models, the representation of clouds on a coarse grid resolution is subordinate to the small-scale parameterization schemes employed, attempting to account for the full range of scales involved therein (Zelinka et al., 2016; Zelinka et al., 2020).

Besides the uncertainties tied to observations and modeling, the sensitivity of clouds to temperature patterns (Zhou et al., 2016) and other large-scale climate drivers (Gulev et al., 2021) can also lead to discrepancies between estimations of cloud coverage trends over different periods and regions. One example is found in the El Niño-Southern Oscillation (ENSO), a dominant mode of climate variability with seasonal-to-interannual time scales, traditionally emerging over the Tropical Pacific Ocean (Neelin et al., 1998). Through the strong coupling between the Pacific Ocean and the atmosphere above, ENSO's impact goes beyond the Pacific (Taschetto et al., 2020) and modulates global temperatures and cloud features (Davey et al., 2014; Yang et al., 2016). Thus, the ENSO signal often stands out as a major driver of variability in climate records, blurring the global-warming related trend, and even biasing its magnitude on decadal time scales (Compo and Sardeshmukh, 2010) due to the ENSO's low-frequency variability (Hope et al., 2017). Similarly, other large-scale climate phenomena, such as the Atlantic Multi-decadal Oscillation and the Pacific Decadal Oscillation, are natural climate variability candidates that perturb global temperatures (Deser et al., 2010) and cloud coverage (Li et al., 2021). Therefore, they may introduce additional bias into global-warming related trends.

To avoid these potential obstacles, we analyze modes of variability in global cloud coverage by performing an Empirical Orthogonal Function (EOF) decomposition on 42 years (1979–2020) of ERA5 data (Hersbach et al., 2020); see Sec. 2. To set the stage and to have a well-studied reference, we analyze the global Skin Temperature (ST) together with the Total Cloud Cover (TCC). ST, in ERA5, is the theoretical temperature of the Earth's surface required to satisfy the surface energy balance, and TCC is the part of a grid box covered by clouds.

2 Materials and Methods

1.1 Dataset

This study uses the 42 years (1979–2020) of monthly Atmospheric data from the European Centre for Medium-Range Weather Forecasts Reanalysis, Version 5 (ERA5, https://www.ecmwf.int/en/forecasts/datasets/reanalysis-datasets/era5, Hersbach et al., 2020), with a horizontal resolution of 0.25 °. ERA5 has been validated as the most reliable reanalysis dataset for climate trend assessment (Gulev et al., 2021). The cloud cover in ERA5 is calculated using thermodynamic conditions that are optimally constrained by state-of-the-art observations, providing uniformly sampled, long-term data of high-quality estimates (Hersbach

https://doi.org/10.5194/acp-2022-817
Preprint. Discussion started: 19 December 2022

Atmospheric Chemistry and Physics Discussions

et al., 2019). In particular, the calculated TCC was shown to be in good agreement with the spatiotemporal characteristics of measured cloud coverages (Yao et al., 2020).

1.2 Data Processing

Apart from the calculation of the Oceanic Niño Index (ONI), the entire analysis is based on annual data and anomalies. The annual data is calculated as a simple average of monthly data for each calendar year. The annual anomaly is the deviation of the annual data from the mean over 1979–2020. For the ONI calculation, we used the monthly ST anomaly. It is calculated as the deviation of the monthly ST-value from the mean of each given month over 1979–2020.

Near-Surface Relative Humidity (RH_{NS}) is defined here as the Relative Humidity (RH) at 950 hPa over the ocean and at 50 hPa above surface over land. This estimation is based on the RH-values at 23 pressure levels (200, 225, 250, 300, 350, 400, 450, 500, 550, 600, 650, 700, 750, 775, 800, 825, 850, 875, 900, 925, 950, 975, and 1000 hPa). The oceanic and continental grid boxes are identified by a Land-Sea Mask (LSM, the fraction of land, as opposed to the ocean or inland waters, in a grid box) from ERA5. A grid box with an LSM-value ≤ 0.2 is considered oceanic, and its RH_{NS} value is given as the RH at 950 hPa. A grid box with a LSM-value larger than 0.2 is considered continental, and its RH_{NS} value is calculated using the values at the adjacent pressure levels by a pressure-difference weighted linear interpolation. The pressure values at those layers are calculated by monthly surface pressure data from ERA5.

1.3 Area and TCC Weighting

Since the area of each 0.25 ° by 0.25 ° grid box, as used in this study, depends on latitude, we performed an area weighting for all spatial averages. The area of each grid box is calculated as the product of arc lengths at the corresponding latitude and longitude by regarding the Earth as an oblate spheroid with a radius of 6378.137 km at the equator and 6356.752 km at the poles. In addition, we performed a TCC weighting to account for the spatial dependence of cloud coverage when assessing cloud-related processes. The weights are given in Fig. 1c.

1.4 EOF Analysis

EOF analysis is a decomposition approach that is widely used in meteorology and oceanography (Lorenz, 1956; Preisendorfer and Mobley, 1988). It decomposes any given spatiotemporal field into a set of independent EOF modes in the spatial domain whose temporal variations are encoded by the corresponding Principal Components (PCs). With the proper interpretations, these independent modes can provide important clues about the physics and dynamics of the investigated system (Schnur et al., 1993; Dunkerton, 1993; Dror et al., 2021). More specifically, EOFs and PCs come in pairs and are ordered by the corresponding variance that is explained by each given mode. The number of EOF-PC pairs is determined by the temporal dimension of the input data (42 for the annual ST and TCC anomalies considered here).

In this study, we used area-weighted data for the EOF analysis of annual ST and TCC anomalies to isolate the main drivers of global surface temperature and cloud coverage. The area weighting is required in order to lessen the contribution of smaller-

https://doi.org/10.5194/acp-2022-817
Preprint. Discussion started: 19 December 2022


Atmospheric Chemistry and Physics Discussions

size grid boxes (Baldwin et al., 2009). Once the EOF analysis is performed on the area-weighted ST and TCC data, the final EOF modes presented in the main text are rescaled by dividing them by the corresponding area weights. The underlying EOF analysis is performed using the Python library, eofs (Version 1.4.0, https://github.com/ajdawson/eofs, Dawson, 2016).

1.5 ONI

ONI is defined as the 3-month running mean of sea surface temperature anomaly over the Niño3.4 region (5° N–5° S and 170° W–120° W). It provides a common measure of the state of ENSO (Glantz and Ramirez, 2020). Large positive ONI-values indicate strong warm phases of ENSO (El Niño, the unusual increase in sea surface temperature over the central and Eastern tropical Pacific Ocean), whereas large negative ONI-values correspond to strong cold phases of ENSO (La Niña, the cold counterpart of El Niño). Here, to link EOF modes for ST and TCC with known physical processes, such as ENSO, we calculate the ONI as the area-weighted mean of monthly ST anomalies over the Niño3.4 region.

1.6 Spearman's Correlation Coefficient (Spearman's ρ)

Spearman's ρ is a nonparametric statistical measure of the strength of a monotonic relationship between two ranked variables. Spearman's ρ ranges between -1 and 1, while 0 implies an absence of correlation, and proximity to +/-1 ρ-values implies a stronger monotonic relationship. In this study, we calculate Spearman's ρ between different variables to measure their correlation. Since we are after correlations of interest in both negative and positive directions, we performed a two-tailed t-test with a 95 % confidence interval (p-values < 0.05) to assess the statistical significance. For the computation of Spearman's ρ and p-values, we used the Python library, SciPy (Version 1.5.2, https://scipy.org/).

3 Results

Figures 1a and 1c show the geographical distributions of annual mean ST and TCC data, averaged over the period 1979–2020. It reveals the nearly uniform temperature gradient towards the poles and the expected patterns of high cloud coverage over the tropics and marine mid-latitudes and the extremely low cloud coverage over the deserts. Figures 1b and 1d plot the area-weighted global mean of annual ST and TCC data; see Sec. 2. The observed increasing ST trend represents clear evidence of global warming (Eyring et al., 2021). In contrast, the evident lack of a consistent trend in TCC suggests that perturbations other than a warming climate might dominate the TCC variability.

To identify and isolate the main underlying drivers in the observed variations, we perform an area-weighted EOF analysis on annual ST and TCC anomalies; see Sec. 2. The results reveal Spatio-temporal fields sufficient for identifying modes of variability driven by distinct physical processes. For each analyzed variable, these results exhibit spatial patterns captured by EOF modes, whose temporal variations are encoded by the corresponding PC (Lorenz, 1956). By analyzing the PC's time-variability, we are able to find correspondences between the EOF modes and known climate phenomena (Preisendorfer and Mobley, 1988). Notably, unlike EOF modes, physical processes are not necessarily orthogonal, and variations caused by one

https://doi.org/10.5194/acp-2022-817
Preprint. Discussion started: 19 December 2022


Atmospheric Chemistry and Physics Discussions

physical process could be split into different EOF modes, a phenomenon known as signal leakage (Richman, 1986). However, this issue is negligible for the dataset at hand, in particular for the dominant EOF modes of ST and TCC discussed below; see fig. S1 and Supplementary Text 1.

To set the stage, we first present our findings for the global surface temperature. Figure 2 shows the two dominant EOF modes of the annual ST anomaly along with their PCs. Recall that a given PC encodes the temporal variability captured by the corresponding EOF mode, whose spatial features specify, in turn, the magnitude and direction of the PC over each region. For the dataset at hand, the leading EOF mode of ST (EOF1, Fig. 2a) accounts for 28.3 % of the total variance and distills a consistent warming trend (PC1, Fig. 2b) over nearly all continents and most oceans (red shades in Fig. 2a). Its PC evolves almost synchronously with the annual global mean ST (black curve in Fig. 2b).

This leading EOF mode reveals some regional features of the recent warming climate, such as the most significant warming being over the Arctics (Serreze and Barry, 2011), the nearly twice larger warming rate over land than over the ocean (Byrne and O'Gorman, 2018), and the feeble warming or even cooling signal over parts of the North Atlantic Ocean, the southeast Pacific Ocean, and the Southern Ocean (Keil et al., 2020; Heede and Fedorov, 2021; Bintanja et al., 2013). These features highlight that regional feedbacks can modify the warming pattern and lead to non-uniform warming.

The second component of ST variations (EOF2, Fig. 2c), accounting here for 11.1 % of the total variance, manifests itself as an ENSO-associated mode. This feature becomes strikingly apparent when comparing its PC (PC2, Fig. 2d) with the ONI, a common measure of ENSO (Glantz and Ramirez, 2020); see the black curve in Fig. 2d and Sec. 2. An episode of large positive values in PC2 coincides with large positive ONI-values, indicative of El Niño events. Analogously, episodes of large negative values for this PC2 coincide with large negative ONI-values, corresponding to La Niña events (Neelin et al., 1998).

As expected, EOF2 for ST shows strong positive anomalies over the central and Eastern tropical Pacific and negative anomalies over the Western Pacific. Furthermore, beyond the Pacific Ocean, ST over areas with strong negative (e.g., North America and the adjacent North Atlantic Ocean) and positive (e.g., South Africa, parts of Asia, Australia, and a part of the Southern Ocean) anomalies also closely correlate to ENSO events. These findings are consistent with previous studies (Deser et al., 2010; Davey et al., 2014) and highlight ENSO as an essential driver of the global climate system (Taschetto et al., 2020).

Overall, the EOF analysis for ST demonstrates that the global warming trend and ENSO are the dominant factors in surface temperature variability over the last 42 years. We turn next to our EOF results of global cloud coverage. Figure 3 presents the two dominant EOF modes and the corresponding PCs of the annual TCC anomaly. The first thing to note is that similarly to ST findings, a trend and an ENSO-associated mode are identified but in opposite order. The EOF1 for TCC (Fig. 3a) shows an ENSO-associated behavior with its PC (Fig. 3b), evolving almost in perfect synchrony with the ONI. While EOF2 (Fig. 3c) demonstrates a clear trend with its PC (Fig. 3d), which strongly correlates with the annual global mean ST (black curve in Fig. 3d; Spearman's $\rho = 0.86$, p-value $= 1.65\times10^{-13}$, two-tailed t-test, see Sec. 2).

This EOF1 for TCC shows that the global cloud coverage is greatly influenced by ENSO and accounts for 21.8 % of the total variance. It suggests that maritime Southeast Asia and the Western Pacific are anti-correlated with the PC and hence the ONI (blue shades in Fig. 3a). Consequently, the cloud coverage in regions of positive anomalies over the central to eastern Pacific

https://doi.org/10.5194/acp-2022-817
Preprint. Discussion started: 19 December 2022


Atmospheric Chemistry and Physics Discussions

(red shades in Fig. 3a) will decrease during El Niño years and increase during La Niña years, and vice versa. Beyond the Pacific Ocean, the analysis reveals strong negative correlations over the tropical Atlantic Ocean and positive correlations over western Asia, part of South Africa, the Southern United States, and the adjacent North Pacific Ocean. The patterns revealed here are consistent with satellite observations for the ENSO forced precipitation tendency (Davey et al., 2014). Moreover, they agree well with previous studies showing similar ENSO-associated modes in cloud radiative effects and cloud coverage by simulations and corrected satellite records (Yang et al., 2016; Li et al., 2021).

After decoupling the ENSO-associated mode from TCC, a clear trend mode (Fig. 3c) appears. This trend mode in TCC accounts for 14.4 % of the total variance and yields a PC evolving similarly to the one associated with the observed ST warming mode; see Fig. 2b. However, unlike the latter, whose warming pattern is expressed throughout the globe, patterns of TCC growth are observed over a major part of the ocean (red shades in Fig. 3c), while patterns corresponding to shrinking TCC occur over most of the continents (blue shades in Fig. 3c). More specifically, the tropical and subtropical oceans exhibit the most significant increasing trends; while for the continents, South and North America, the Congo Basin, most of Asia, Europe, and the poles exhibit a clear decreasing trend, the desert areas and the Indian subcontinent tend to display an increasing trend. The reported trends agree with some previously-made estimations using historical observations (Warren et al., 2007; Zhou et al., 2016; Norris et al., 2016). However, there is some contradiction with model-based future-climate prediction studies, which suggested a decrease in marine stratocumulus cloud coverage in warmer climate conditions (Forster et al., 2021; Zelinka et al., 2016).

Relying on the EOF analysis, we observe a clear signature of the warming climate on global cloud coverage. We explore next the thermodynamic drivers that could explain the observed TCC trend. In that respect, we assess the correlation between each ERA5 meteorological variable (207 in total) and TCC by calculating the corresponding Spearman's ρ for the annual data. Meteorological variables that are checked here include RH, Specific Humidity (SH), Temperature (T), U-wind component (U), V-wind component (V), vertical velocity (ω), wind divergence (Div), Potential Vorticity (PV), and Relative Vorticity (RV) at 23 pressure levels ranging from 200 to 1000 hPa, see Sec. 2.

Figure 4a presents the averaged correlations over land and ocean; see Sec. 2. It is evident that RH in most of the pressure levels yields the strongest correlation with continental TCC, while for maritime TCC, RH and SH yield comparably strong correlations. A previous analysis based on satellite observations and other atmospheric reanalysis datasets obtained similar conclusions (Koren et al., 2010). The geographical distribution of the meteorological variables that best correlate with TCC, shown in Fig. 4b, further highlights RH as the strongest component over almost all continents. Moreover, there is no single variable besides RH that correlates strongly with nearly all continental TCC; see Fig. S2 and Supplementary Text 2. As for the maritime TCC, it exhibits a diversity of variables dominated by relative and specific humidities.

The RH correlation score shows a global peak over land (0.65±0.20) and a local peak over the ocean (0.43±0.22) slightly above the surface (925 hPa, the magenta arrow in Fig. 4a). RH, which, for a given pressure level, is a function of the specific humidity and the temperature, is a key parameter in determining cloud properties. Based on a parcel's theory describing convective cloud formation, the low-level RH will determine the likelihood of cloud formation and its extent. Moreover, low-level RH represents

https://doi.org/10.5194/acp-2022-817
Preprint. Discussion started: 19 December 2022


Atmospheric Chemistry and Physics Discussions

a more localized process, while high-level RH-values are likely to be affected by processes such as cloud evaporation and long-distance water vapor transport (Bengtsson, 2010). Therefore, to further explore the links between TCC and RH, we introduce a hybrid RH variable denoted as the near-surface RH (RH_{NS}), taking into account the terrestrial topography. RH_{NS} is defined as RH at 950 hPa over the ocean, and the RH at a pressure level of 50 hPa less than the local surface pressure over land, see Sec. 2.

Figure 5a shows the temporal trend in RH_{NS} for the study duration (1979–2020) using ordinary least-square regression analysis (Wells and Krakiwsky, 1971). It shows a clear, consistent decreasing trend in RH_{NS} over land at a rate of 1–2 % decade^{-1}, as well as similar spatial patterns in these RH_{NS} trends to those exhibited in the TCC trend mode. The larger decreasing rate of RH_{NS} over the continents is expected due to the limited reservoir of water vapor and the larger warming rate over land; see Fig. 2a. Figure 5b shows a map of the correlation between RH_{NS} and TCC, revealing a distinct contrast between the high correlation scores for most of the continents (apart from the Sahara) compared to the oceans. The distributions of the correlations (Fig. 5c) show the high and relatively narrow correlation spread over land. Moreover, the global mean correlation of TCC with RH_{NS} shows the highest score of 0.69±0.18 over land.

4 Discussion

Surface temperature is likely to be the most explored variable with respect to climate change (Gulev et al., 2021). It is a direct measure of global warming on the most relevant level for most biological systems, and it characterizes the temperature interface between the ocean and land, and the atmosphere. As such, it sets boundary conditions for tropospheric processes. Clouds are at the heart of the water cycle and serve as the radiation modulators of the atmosphere (Bengtsson, 2010; Stephens et al., 2012). Though the overall effects on the fresh water and radiative budgets depend on cloud type and properties (Chen et al., 2000; Houze, 2014), the first variable to explore is the horizontal cloud extent, namely what fraction of the sky that is cloudy per each region on the globe.

By performing EOF analysis on ERA5 data over 1979–2020, we showed that the two dominant modes of surface temperature and the total cloud coverage can be described as a trend and an ENSO tendency. The order of these modes is flipped; for the surface temperature, the trend leads the ENSO, while for cloud coverage, the trend follows the ENSO.

We used the frequently-explored surface temperature data to set the stage and demonstrate the rich information that can be drawn from the modes. The temperature analysis yields a clear trend captured by the leading PC paired with an almost totally red EOF mode (i.e., dominated by positive anomalies) of known regional features (Serreze and Barry, 2011; Byrne and O'Gorman, 2018; Keil et al., 2020; Heede and Fedorov, 2021; Bintanja et al., 2013). The second mode reveals a rich pattern of ENSO weights and signs over the entire globe, highlighting the fact that ENSO is a key driver of the global climate system (Neelin et al., 1998; Taschetto et al., 2020). The cloud coverage analysis shows a clear ENSO mode followed by a trend mode in terms of variance decomposition. The complex sensitivity of cloud coverage to ENSO could partly explain why it is

https://doi.org/10.5194/acp-2022-817
Preprint. Discussion started: 19 December 2022


Atmospheric Chemistry and Physics Discussions

challenging to find climate trends in clouds. The trend mode shows growth in cloud coverage with time over the tropical and subtropical oceans, while shrinking in cloud coverage is observed over most non-desert continents.

Because of the limited availability of water vapor sources over land, terrestrial clouds are more likely to be humidity-limited. Relative humidity measures how far a given specific humidity is from saturation per given temperature and pressure and is, therefore, a fundamental measure of cloud formation. In particular, relative humidity near the surface dictates the initial conditions of a rising air parcel. In a warming climate, over the continents, near-surface relative humidity is expected to decline (Byrne and O'Gorman, 2018) and is likely to affect cloud formation similarly. Over the warming oceans, for which the water vapor reservoir is not limited, enhanced evaporation can supply additional water vapor. Therefore, trends of near-surface relative humidity and their links to cloud coverage over the oceans are less distinct.

Our results have several implications. The more optimistic one is that increased cloud coverage over the central belt of the oceans implies a possible negative cloud feedback to global warming. The total effect will subsequently depend on how the increased cloud coverage is distributed among cloud types and their properties. Nevertheless, as a first approximation, larger subtropical marine stratocumulus decks are likely to cause stronger cooling (Wood, 2012; Zelinka et al., 2017). In contrast, the consistent reduction in cloud coverage over land suggests an additional warming and larger stress on the freshwater supply that is already in shortage in many regions around the globe (Oki and Kanae, 2006). In particular, the decrease in cloud coverage over the Amazon and Congo Basins, which contain the largest rainforests and the most precious and vulnerable ecosystems on our planet, is especially disconcerting (Langenbrunner et al., 2019; Bush et al., 2011; Lenton, 2011). Moreover, such a contrast in cloud trends between land and ocean (Fig. 3c) suggests changes in the radiative energy partitioning between the two media that might ignite additional feedbacks and changes in the atmospheric circulation.

Supplementary information

Supplementary Text 1–2
Figures S1–2

Code and data availability

All analysis is conducted by the programming language, Python (Version 3.7.0, https://www.python.org/). All data, documentation, and programming library used in analysis are publicly available (see websites in Sec. 2.).

Author contribution

I.K. and H.L. designed the study. H.L. conducted the data analysis. O.A., I.K., H.L., and M.D.C. wrote the manuscript. All co-authors provided critical feedback and helped shape the research, conceptualization, investigation, and manuscript.

https://doi.org/10.5194/acp-2022-817
Preprint. Discussion started: 19 December 2022

Atmospheric Chemistry and Physics Discussions

Competing interests

The authors declare that they have no conflict of interest.

Acknowledgments

This work has been supported by the European Research Council (ERC) under the European Union's Horizon 2020 research and innovation program (grant agreement No. 810370). This study was also partly supported by a Ben May Center grant for theoretical and/or computational research and by the Israeli Council for Higher Education (CHE) via the Weizmann Data Science Research Center.

References

Aerenson, T., Marchand, R., Chepfer, H., and Medeiros, B.: When will MISR detect rising high clouds?, Journal of Geophysical Research: Atmospheres, 127, 2021–035865, doi.org/10.1029/2021JD035865, 2022.

Baldwin, M.P., Stephenson, D.B., and Jolliffe, I.T.: Spatial weighting and iterative projection methods for eofs, Journal of Climate, 22, 234–243, doi.org/10.1175/2008J, 2009.

Bengtsson, L.: The global atmospheric water cycle, Environmental Research Letters, 5, 025202, doi.org/10.1088/1748-9326/5/2/025002, 2010.

Bintanja, R., van Oldenborgh, G.J., Drijfhout, S., Wouters, B., and Katsman, C.: Important role for ocean warming and increased ice-shelf melt in antarctic sea-ice expansion, Nature Geoscience, 6, 376–379, doi.org/10.1038/ngeo1767, 2013.

Bush, M., Flenley, J., and Gosling, W.: Tropical Rainforest Responses to Climatic Change, Springer, Chichester, 2011.

Byrne, M.P. and O'Gorman, P.A.: Trends in continental temperature and humidity directly linked to ocean warming, Proceedings of the National Academy of Sciences, 115, 4863–4868, doi.org/10.1073/pnas.172231211, 2018.

Ceppi, P., Brient, F., Zelinka, M.D., and Hartmann, D.L.: Cloud feedback mechanisms and their representation in global climate models, Wiley Interdisciplinary Reviews: Climate Change, 8, 465, doi.org/10.1002/wcc.465, 2017.

Chen, T., Rossow, W.B., and Zhang, Y.: Radiative effects of cloud-type variations, Journal of climate, 13, 264–286, doi.org/10.1175/1520-0442(2000)013⟨ 0264:REOCTV⟩ 2.0.CO;2, 2000.

Chepfer, H., Noel, V., Winker, D., and Chiriaco, M.: Where and when will we observe cloud changes due to climate warming?, Geophysical Research Letters, 41, 8387–8395, doi.org/10.1002/2014GL061792, 2014.

Compo, G.P. and Sardeshmukh, P.D.: Removing ENSO-related variations from the climate record. Journal of Climate, 23, 1957–1978, doi.org/10.1175/2009JCLI2735.1, 2010.

Davey, M., Brookshaw, A., and Ineson, S.: The probability of the impact of ENSO on precipitation and near-surface temperature, Climate Risk Management, 1, 5–24, doi.org/10.1016/j.crm.2013.12.002, 2014.

https://doi.org/10.5194/acp-2022-817
Preprint. Discussion started: 19 December 2022


Atmospheric Chemistry and Physics Discussions

Dawson, A.: Eofs: a library for eof analysis of meteorological, oceanographic, and climate data. Journal of Open Research Software, 4, doi.org/10.5334/jors.122, 2016.

Deser, C., Alexander, M.A., Xie, S.-P., and Phillips, A.S.: Sea surface temperature variability: patterns and mechanisms. Annu. Rev. Mar. Sci, 2, 115–143, doi.org/10.1146/annurev-marine-120408-151453, 2010.

Dror, T., Chekroun, M.D., Altaratz, O., and Koren, I.: Deciphering organization of goes-16 green cumulus through the empirical orthogonal function (eof) lens, Atmospheric chemistry and physics, 21, 12261–12272, doi.org/10.5194/acp-21-12261-2021, 2021.

Dunkerton, T.J.: Observation of 3–6-day meridional wind oscillations over the tropical pacific, 1973–1992: vertical structure and interannual variability, Journal of Atmospheric Sciences, 50, 3292–3307, doi.org/10.1175/1520-0469(1995)052⟨ 1585:OODMWO⟩ 2.0.CO;2, 1993.

Eastman, R., Warren, S.G., and Hahn, C.J.: Variations in cloud cover and cloud types over the ocean from surface observations, 1954–2008. Journal of Climate, 24, 5914–5934, doi.org/10.1175/2011JCLI3972.1, 2011.

Evan, A.T., Heidinger, A.K., and Vimont, D.J.: Arguments against a physical long-term trend in global ISCCP cloud amounts, Geophysical Research Letters, 34, doi.org/10.1029/2006GL028083, 2007.

Eyring, V., Gillett, N.P., Achuta Rao, K.M., Barimalala, R., Barreiro Parrillo, M., Bellouin, N., Cassou, C., Durack, P.J., Kosaka, Y., McGregor, S., Min, S., Morgenstern, O., and Sun, Y.: In: Masson-Delmotte, V., Zhai, P., Pirani, A., Connors, S.L., Pean, C., Berger, S., Caud, N., Chen, Y., Goldfarb, L., Gomis, M.I., Huang, M., Leitzell, K., Lonnoy, E., Matthews, J.B.R., Maycock, T.K., Waterfield, T., Yelekci, O., Yu, R., and Zhou, B. (eds.) Human influence on the climate system, pp. 423–552. Cambridge University Press, Cambridge, United Kingdom and New York, NY, USA, doi.org/10.1017/9781009157896.005, 2021.

Forster, P., Storelvmo, T., Armour, K., Collins, W., Dufresne, J.-L., Frame, D., Lunt, D.J., Mauritsen, T., Palmer, M.D., Watanabe, M., Wild, M., and Zhang, H.: In: Masson-Delmotte, V., Zhai, P., Pirani, A., Connors, S.L., Pean, C., Berger, S., Caud, N., Chen, Y., Goldfarb, L., Gomis, M.I., Huang, M., Leitzell, K., Lonnoy, E., Matthews, J.B.R., Maycock, T.K., Waterfield, T., Yelekci, O., Yu, R., Zhou, B. (eds.): The Earth's energy budget, climate feedbacks, and climate sensitivity, pp. 923–1054. Cambridge University Press, Cambridge, United Kingdom and New York, NY, USA. doi.org/10.1017/9781009157896.009, 2021.

Gettelman, A., and Sherwood, S.C.: Processes responsible for cloud feedback, Current climate change reports, 2, 179–189, doi.org/10.1007/s40641-016-0052-8, 2016.

Glantz, M.H. and Ramirez, I.J.: Reviewing the oceanic Nino index (ONI) to enhance societal readiness for El Nino's impacts, International Journal of Disaster Risk Science, 11, 394–403, doi.org/10.1007/s13753-020-00275-w, 2020.

Gulev, S.K., Thorne, P.W., Ahn, J., Dentener, F.J., Domingues, C.M., Gerland, S., Gong, D., Kaufman, D.S., Nnamchi, H.C., Quaas, J., Rivera, J.A., Sathyendranath, S., Smith, S.L., Trewin, B., von Schuckmann, K., and Vose, R.S.: In: Masson-Delmotte, V., Zhai, P., Pirani, A., Connors, S.L., Pean, C., Berger, S., Caud, N., Chen, Y., Goldfarb, L., Gomis, M.I., Huang, M., Leitzell, K., Lonnoy, E., Matthews, J.B.R., Maycock, T.K., Waterfield, T., Yelekci, O., Yu, R., and Zhou, B. (eds.)

https://doi.org/10.5194/acp-2022-817
Preprint. Discussion started: 19 December 2022


Atmospheric Chemistry and Physics Discussions

Changing state of the climate system, pp. 287–422. Cambridge University Press, Cambridge, United Kingdom and New York, NY, USA, doi.org/10.1017/9781009157896.004, 2021.

Heede, U.K. and Fedorov, A.V.: Eastern equatorial pacific warming delayed by aerosols and thermostat response to co2 increase, Nature Climate Change, 11, 696–703, doi.org/10.1038/s41558-021-01101-x, 2021.

Hersbach, H., Bell, B., Berrisford, P., Biavati, G., Horanyi, A., Munoz Sabater, J., Nicolas, J., Peubey, C., Radu, R., Rozum, I., et al.: Era5 monthly averaged data on single levels from 1979 to present, Copernicus Climate Change Service (C3S) Climate Data Store (CDS) 10, 252–266, doi.org/10.24381/cds.f17050d7, 2019.

Hersbach, H., Bell, B., Berrisford, P., Hirahara, S., Horanyi, A., Munoz-Sabater, J., Nicolas, J., Peubey, C., Radu, R., Schepers, D., Simmons, A., Soci, C., Abdalla, S., Abellan, X., Balsamo, G., Bechtold, P., Biavati, G., Bidlot, J., Bonavita, M., Chiara, G.D., Dahlgren, P., Dee, D., Diamantakis, M., Dragani, R., Flemming, J., Forbes, R., Fuentes, M., Geer, A., Haimberger, L., Healy, S., Hogan, R.J., Holm, E., Janiskov, M., Keeley, S., Laloyaus, P., Lopez, P., Lupu, C., Radnoti, G., Rosnay, P.D., Rozum, I., Vamborg, F., Villaume, S., and Thepaut, J.–N.: The ERA5 global reanalysis. Quarterly Journal of the Royal Meteorological Society, 146, 1999–2049, doi.org/10.1002/qj.3803, 2020.

Hope, P., Henley, B.J., Gergis, J., Brown, J., and Ye, H.: Time-varying spectral characteristics of ENSO over the last millennium. Climate Dynamics, 49, 1705–1727, doi.org/10.1007/s00382-016-3393-z, 2017.

Houze Jr, R.A.: Cloud Dynamics, Academic press, Oxford UK, 2014.

Karlsson, K.-G., and Devasthale, A.: Inter-comparison and evaluation of the four longest satellite-derived cloud climate data records: Clara-a2, esa cloud cci v3, isccp-hgm, and patmos-x, Remote Sensing, 10, 1567, doi.org/10.3390/rs10101567, 2018.

Keil, P., Mauritsen, T., Jungclaus, J., Hedemann, C., Olonscheck, D., and Ghosh, R.: Multiple drivers of the north Atlantic warming hole. Nature Climate Change, 10, 667–671, doi.org/10.1038/s41558-020-0819-8, 2020.

Koren, I., Feingold, G., and Remer, L.A.: The invigoration of deep convective clouds over the atlantic: aerosol effect, meteorology or retrieval artifact?. Atmospheric Chemistry and Physics, 10, 8855–8872, doi.org/10.5194/acp-10-8855-2010, 2010.

Langenbrunner, B., Pritchard, M., Kooperman, G.J., and Randerson, J.T.: Why does amazon precipitation decrease when tropical forests respond to increasing co2?, Earth's future, 7, 450–468, doi.org/10.1029/2018EF001026, 2019.

Lenton, T.M.: Early warning of climate tipping points, Nature climate change, 1, 201–209, doi.org/10.1038/nclimate1143, 2011.

Li, Y., Ge, J., Dong, Z., Hu, X., Yang, X., Wang, M., Han, Z.: Pairwise-rotated eofs of global cloud cover and their linkages to sea surface temperature. International Journal of Climatology, 41, 2342–2359, doi.org/10.1002/joc.6962, 2021.

Lorenz, E.N.: Empirical Orthogonal Functions and Statistical Weather Prediction, Massachusetts Institute of Technology, Department of Meteorology Cambridge, Cambridge Massachusetts, 1, 1956.

Neelin, J.D., Battisti, D.S., Hirst, A.C., Jin, F.-F., Wakata, Y., Yamagata, T., and Zebiak, S.E.: ENSO theory, Journal of Geophysical Research: Oceans, 103, 14261–14290, doi.org/10.1029/97JC03424, 1998.

https://doi.org/10.5194/acp-2022-817
Preprint. Discussion started: 19 December 2022


Atmospheric Chemistry and Physics Discussions

345 Norris, J.R., and Evan, A.T.: Empirical removal of artifacts from the isccp and patmos-x satellite cloud records, Journal of Atmospheric and Oceanic Technology, 32, 691–702, doi.org/10.1175/JTECH-D-14-00058.1, 2015.

Norris, J.R., Allen, R.J., Evan, A.T., Zelinka, M.D., O'Dell, C.W., and Klein, S.A.: Evidence for climate change in the satellite cloud record. Nature, 536, 72–75, doi.org/10.1038/nature18273, 2016.

Oki, T. and Kanae, S.: Global hydrological cycles and world water resources, science, 313, 1068–1072,
350 doi.org/10.1126/science.1128845, 2006.

Preisendorfer, R.W., and Mobley, C.D.: Principal component analysis in meteorology and oceanography, Developments in atmospheric science, 17, 1988.

Richman, M.B.: Rotation of principal components, Journal of climatology, 6, 293–335, doi.org/10.1002/joc.3370060305, 1986.

355 Schnur, R., Schmitz, G., Grieger, N., and Von Storch, H.: Normal modes of the atmosphere as estimated by principal oscillation patterns and derived from quasigeostrophic theory, Journal of the atmospheric sciences, 50, 2386–2400, doi.org/10.1175/1520-0469(1993)050⟨ 2386:NMOTAA⟩ 2.0.CO;2, 1993.

Serreze, M.C. and Barry, R.G.: Processes and impacts of arctic amplification: a research synthesis, Global and planetary change, 77, 85–96, doi.org/10.1016/j.gloplacha.2011.03.004, 2011.

360 Stephens, G.L., Li, J., Wild, M., Clayson, C.A., Loeb, N., Kato, S., L'ecuyer, T., Stackhouse, P.W., Lebsock, M., and Andrews, T.: An update on earth's energy balance in light of the latest global observations, Nature Geoscience, 5, 691–696, doi.org/10.1038/ngeo1580, 2012.

Stevens, B., ans Bony, S.: What are climate models missing?, Science, 340, 1053–1054, doi.org/10.1126/science.1237554, 2013.

365 Taschetto, A.S., Ummenhofer, C.C., Stuecker, M.F., Dommenget, D., Ashok, K., Rodrigues, R.R., and Yeh, S.-W.: ENSO atmospheric teleconnections, El Nino southern oscillation in a changing climate, 309–335, doi.org/10.1002/9781119548164.ch14, 2020.

Warren, S.G., Eastman, R.M., and Hahn, C.J.: A survey of changes in cloud cover and cloud types over land from surface observations, 1971–96. Journal of climate, 20, 717–738, doi.org/10.1175/JCLI4031.1, 2007.

370 Wells, D.E. and Krakiwsky, E.J.: The Method of Least Squares, Department of Surveying Engineering, University of New Brunswick, Fredericton N.B., 18, 1971.

Wood, R.: Stratocumulus clouds, Monthly Weather Review, 140, 2373–2423, doi.org/10.1175/MWR-D-11-00121.1, 2012.

Yang, Y., Russell, L.M., Xu, L., Lou, S., Lamjiri, M.A., Somerville, R.C., Miller, A.J., Cayan, D.R., DeFlorio, M.J., Ghan, S.J., Liu, Y., Singh, B., Wang, H., Yoon, J.–H., and Rasch, P.J.: Impacts of ENSO events on cloud radiative effects in
375 preindustrial conditions: changes in cloud fraction and their dependence on interactive aerosol emissions and concentrations. Journal of Geophysical Research: Atmospheres, 121, 6321–6335, doi.org/10.1002/2015JD024503, 2016.

Yao, B., Teng, S., Lai, R., Xu, X., Yin, Y., Shi, C., and Liu, C.: Can atmospheric reanalyses (CRA and ERA5) represent cloud spatiotemporal characteristics?. Atmospheric research, 244, 105091, doi.org/10.1016/j.atmosres.2020.105091, 2020.

https://doi.org/10.5194/acp-2022-817
Preprint. Discussion started: 19 December 2022

Zelinka, M.D., Zhou, C., Klein, S.A.: Insights from a refined decomposition of cloud feedbacks, Geophysical Research Letters, 43, 9259–9269, doi.org/10.1002/2016GL069917, 2016.

Zelinka, M.D., Randall, D.A., Webb, M.J., and Klein, S.A.: Clearing clouds of uncertainty, Nature Climate Change, 7, 674–678, doi.org/10.1038/nclimate3402, 2017.

Zelinka, M.D., Myers, T.A., McCoy, D.T., Po-Chedley, S., Caldwell, P.M., Ceppi, P., Klein, S.A., and Taylor, K.E.: Causes of higher climate sensitivity in cmip6 models, Geophysical Research Letters, 47, 2019–085782, doi.org/10.1029/2019GL085782, 2020.

Zhou, C., Zelinka, M.D., and Klein, S.A.: Impact of decadal cloud variations on the earth's energy budget, Nature Geoscience, 9, 871–874, doi.org/10.1038/ngeo2828, 2016.

https://doi.org/10.5194/acp-2022-817
Preprint. Discussion started: 19 December 2022

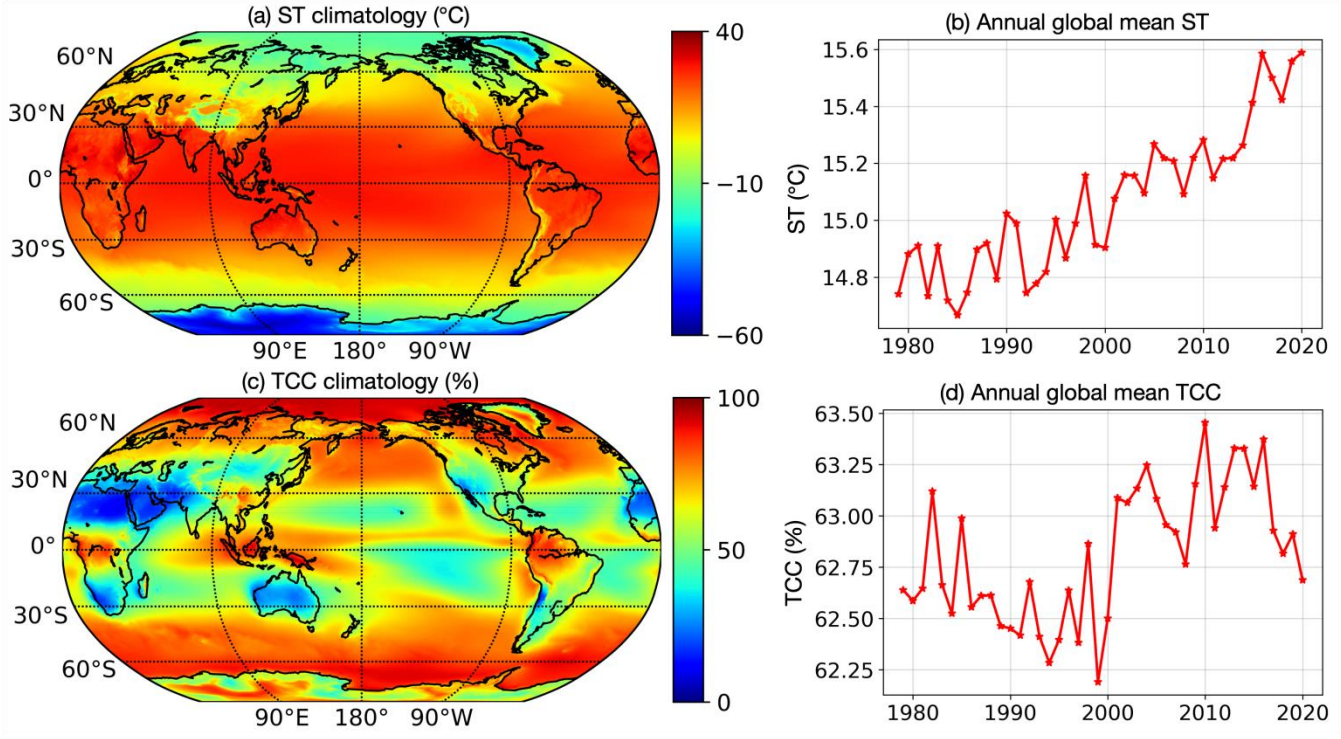

Figure 1: Climatological mean maps and the annual global means (area-weighted) of ST (unit: °C) and TCC (unit: %) during 1979–2020. (a) A global map of the climatological mean of ST. (b) Time series of the annual global mean of ST. (c) A global map of the climatological mean of TCC. (d) Time series of the annual global mean of TCC.

https://doi.org/10.5194/acp-2022-817
Preprint. Discussion started: 19 December 2022

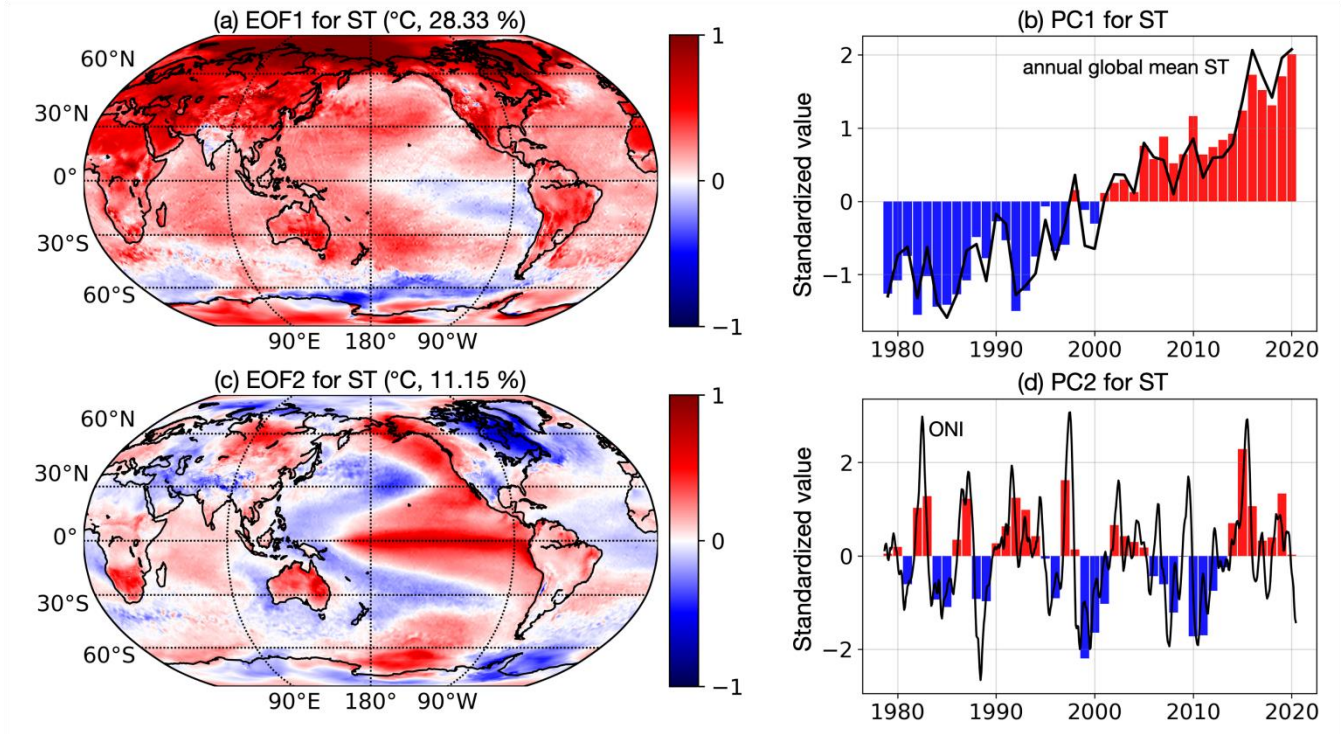

Figure 2: The two dominant EOF modes and their corresponding PCs of the annual ST anomaly (unit: °C) during 1979–2020. (a) The scaled leading EOF mode (EOF1, amplified by the standard deviation of its PC). (b) The standardized leading PC (PC1, divided by its standard deviation). (c) The scaled second EOF mode (EOF2). (d) The standardized second PC (PC2). The black curves in panels b and d are standardized annual global mean ST and ONI. The red and blue bars in panels b and d highlight the positive and negative PC-values, respectively.

https://doi.org/10.5194/acp-2022-817
Preprint. Discussion started: 19 December 2022

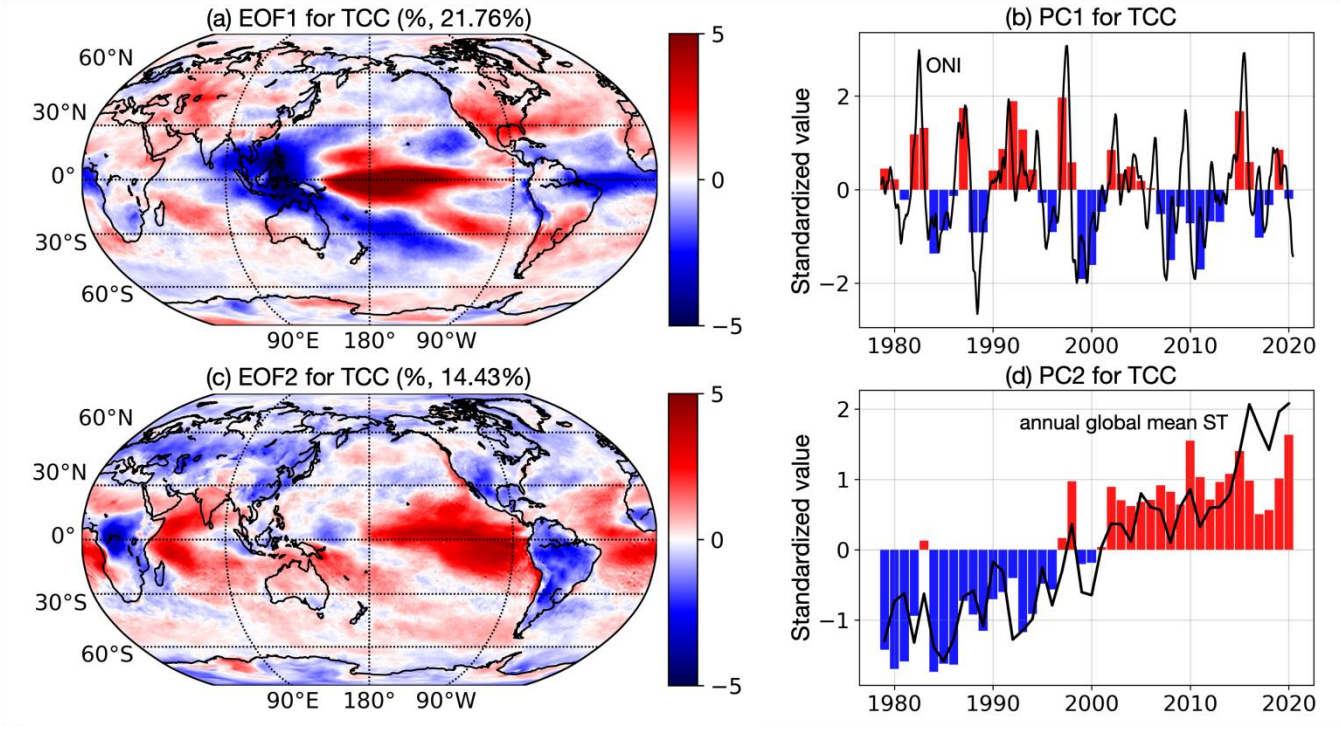

Figure 3: The two dominant EOF modes and their corresponding PCs of the annual TCC anomaly (unit: %) during 1979–2020. (a) The scaled leading EOF mode (EOF1, amplified by the standard deviation of its PC). (b) The standardized leading PC (PC1, divided by its standard deviation). (c) The scaled second EOF mode (EOF2). (d) The standardized second PC (PC2). The black curves in panels b and d are the standardized ONI and annual global mean ST, respectively. The red and blue bars in panels b and d highlight the positive and negative PC values, respectively.

https://doi.org/10.5194/acp-2022-817
Preprint. Discussion started: 19 December 2022

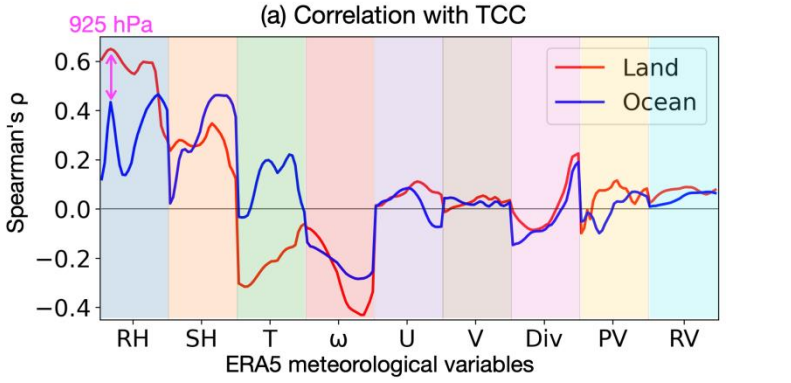

Atmospheric Chemistry and Physics Discussions

405

Figure 4: The relationships between ERA5 meteorological variables and annual TCC during 1979–2020. (a) Averaged Spearman's ρ (area-TCC-weighted) over land and ocean; ρ-values are shown for RH, SH, T, U, V, ω, Div, PV, and RV at 23 pressure levels from 200 to 1000 hPa, starting from near the surface on the left part of the section (light color shades) to the upper atmosphere. (b) Map of the meteorological variables that best correlate with TCC, only Spearman's ρ that are statistically
410 significant at the level of 0.05 (p-value < 0.05, two-tailed t-test) are used.

https://doi.org/10.5194/acp-2022-817
Preprint. Discussion started: 19 December 2022

Atmospheric Chemistry and Physics Discussions

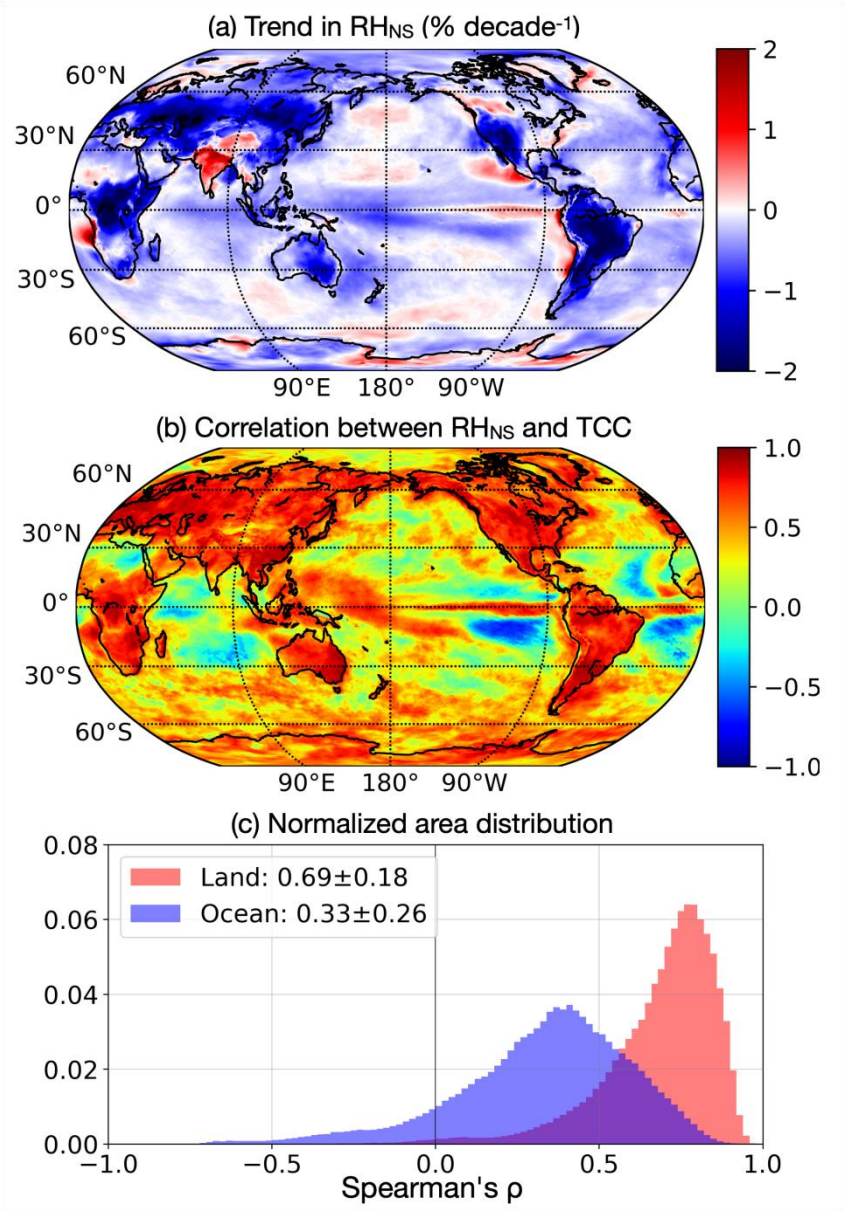

Figure 5: Trends in RH_{NS} and correlations between RH_{NS} and TCC. (a) A map of the temporal trend in annual RH_{NS} (unit: % $decade^{-1}$). (b) A map of Spearman's ρ between RH_{NS} and TCC. (c) Distribution (area-TCC-weighted) of the correlations presented in panel b over land and ocean. The distribution's mean and standard deviation are displayed in the box.